Flexible Coupling Platform for Photonic Integrated Processors

Cátia Pinho[1,2], Berta Neto[1], Tiago M. Morgado[1], Francisco Rodrigues[1,2,3], Ana Tavares[1,2,3], George S. D. Gordon[4], Mário Lima[1,2], Tim D. Wilkinson[4], António Teixeira[1,2]

[1] Instituto de Telecomunicações (IT), University of Aveiro, Portugal
[2] Department of Electronics, Telecommunications and Informatics (DETI), University of Aveiro, Portugal
[3] PICadvanced, Incubadora de Empresas, Universidade de Aveiro, Portugal
[4] Electrical Division, Engineering Department, University of Cambridge, 9, JJ Thomson Avenue, Cambridge, UK
e-mail: catiap@ua.pt, teixeira@ua.pt

***Abstract* — Enhanced Photonic Integrated Circuits (PIC) are required for the current demand of flexibility and reconfigurability in telecommunications networks. However, the technical and functional requirements of the PIC demand a thorough characterization and testing to provide an accurate prediction of the PIC performance. In the characterization and testing context, the use of Spatial Light Modulator (SLM) can be beneficial. SLM is diffractive device to reconstruct images from Computer Generated Holograms (CGH) that allows to modulate the wave form of a light beam. This capability can be explored to feed/receive optical signals to the PIC. In this study, we propose the use of the SLM technology as a flexible coupling platform for photonic integrated processors. Preliminary results were obtained, to produce a multiplexing/demultiplexing CGH to be applied into an optical chip for data compression based on Haar wavelet transform. Simulation results for building blocks as well as the all-optical network for the optical data compression chip are presented, supporting their theoretical feasibility.**

Keywords - Photonic Integrated Circuits (PIC); Integrated Optics; Spatial Light Modulator (SLM); Computer Generated Holography (CGH); All-optical devices; Haar transform .

I. INTRODUCTION

In the recent years, we have witnessed a significant increase in the data traffic which the traditional copper based electronic media fail to carry [1] [2]. Furthermore, the increasing demand for higher image/video storage capacity and data transmission rates led to the search of new bandwidth optimization solutions. Integrated photonics appears as a promising technology to achieve this outcome. Photonic Integrated Circuits (PIC) are the equivalent of Electronic Integrated Circuits (EIC) in the optical domain. As an alternative to transistors and other electronic components, PIC contain optical elements, such as modulators, detectors, attenuators, multiplexers, optical amplifiers and lasers. PIC advantages can be attributed to their lower power consumption, smaller volume and weigh, higher thermal and mechanical stability, and the easier assembly of numerous and complex systems. In sum, PIC-based optical communication systems offer an efficient and cost-effective alternative to data transmission driving to a significant growth in the segment [1]. Furthermore, it is expected an annual growth rate of 25.2% during the estimate period of 2015 to 2022 [2]. PIC increasing demand can also be attributed to innovative applications in bio-photonics [1].

PIC can be characterized as a multiport device composed by an integrated system of optical elements embedded onto a single chip using a waveguide architecture [3]. The testing of optical components is more difficult than on electrical components and for an accurate prediction of the PIC performance, an extensive characterization/testing is required [4]. Moreover, optical components testing is difficult and time-consuming, e.g., due to the tight 3D alignment tolerances for accurate coupling of light [4].

In nowadays demand for data transmission and storage, data compression emerges as an important field of study with different available techniques explored to release additional bandwidth. Specifically, for faster image processing, compression methods are fundamental tools to decrease redundant data. Different compression transformation techniques can be used, with the wavelet-based transforms as the trendiest ones due to their simplicity and fast computation [5]. All-optical network designs appears as a prominent solution for the application of such compression methods. By applying this architecture into a PIC, image compression can be attained with lower cost, less power consumption and high data rate due to an all-optical processing implementation [6]. Among the wavelet-based methods, Haar transform (HT) offers a good approach for image processing and pattern recognition due to its simple design, fast computation power and efficiency, being easily implemented by optical planar interferometry [3], [5], [6]. The HT implementation can be achieved with a two stage network of asymmetric coupler devices [3].

The Spatial Light Modulator (SLM) capability to dynamically reconfigure the light makes it an attractive technology to excite cores and/or modes [7], [8], as it allows the arbitrary addition or removal of channels by the software and it is anticipated that it can improve channel compensation. This feature can then be explored to feed/receive optical signal from PIC.

SLM is an electrically programmable device that modulates light according to a spatial (pixel) pattern [9]. This device can control incident light in amplitude-only, phase-only or the combination phase-amplitude [9], [10]. One of the most commonly used modulation mechanisms is the electro-optical SLM containing liquid crystals as the modulation

material [10], [11]. The liquid crystal spatial light modulators have a microdisplay that is used to collect and modulate the incident light, in a transmissive (liquid crystal display – LCD) or reflective (Liquid Crystal on Silicon – LCoS) form. Another distinguishing characteristic of this modulators is the alignment of the liquid crystal molecules, which is typically either parallel, vertical, or with twisted formation. This determines which variable(s) of the incident light beam can be altered, i.e., phase only, or amplitude and phase [10], [11].

Nonetheless, common hologram generation methods cannot arbitrarily modulate the amplitude and phase of a beam simultaneously [12], [13]. It is not then possible to simply address the inverse Fourier transform of the desired pattern into the far-field and replicate the resulting distribution of amplitude and phase directly on the SLM [12]. Thus, it is necessary to apply optimization algorithms to calculate the best hologram possible within the constraints of the device [12].

The SLM based on nematic LCoS technology is an electrically addressed reflection type phase-only spatial light modulator in which the liquid crystal is controlled by a direct and accurate voltage and can modulate the wave front of a light beam [10], [14], Figure 1.

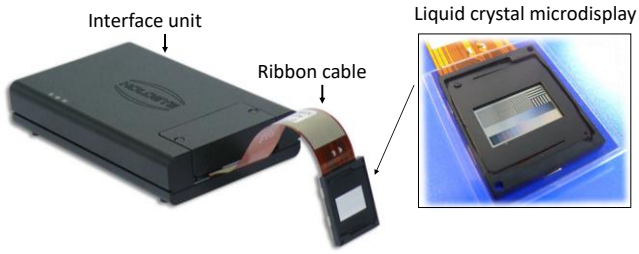

Figure 1. LCOS SLM Pluto phase modulator from Holoeye © 2018 Holoeye Photonics AG.

LCoS SLM is used as a diffractive device to reconstruct images from Computer Generated Holography (CGH) [15]. This optical signal processing can be produced with different techniques, e.g., linear Fourier transform (i.e., linear phase mask) [16], Iterative Fourier Transform Algorithm (IFTA) [17], [18], Gerchberg-Saxton algorithm [19] and simulated annealing [20]. The use of a SLM as a diffractive device to reconstruct images from CGH allows to modulate the wave front of a light beam.

In this study, we proposed the use of the SLM technology as a flexible coupling platform for feeding photonic integrated processors, i.e., to feed/receive optical signal from a PIC. Preliminary results were obtained to produce an expected CGH to be applied into an optical chip for data compression based on Haar wavelet transform.

The paper is organized in four sections. Section II describes the methodology applied. Subsection II-A presents the all-optical system architecture for data compression based in HT; subsection II-B presents the design of the PIC for data compression, addressing the asymmetric coupler and chip design; subsection II-C presents the generation and optimization of the CGH. Section III and IV presents the obtained results and its discussion, respectively. Section V concludes the study.

II. Methodology

The methodology is divided into three subsections: (A) the design of an all-optical system architecture for data compression based in Haar wavelet transform; (B) the algorithms used for the generation and optimization of the CGH; and (C) the implementation of the SLM setup to acquire the CGH.

A. *All-optical system architecture for data compression based in HT*

A digital image can be seen as a group of pixels, where neighboring pixels are correlated and usually redundant. Through the decreasing of this redundancy (by compression techniques) the transmission speed and the bandwidth of the system can be optimized. Transforms based on orthogonal functions are the most frequently used in signal compression techniques. The orthogonality is an important property for multi-resolution analysis, where the original signal can be split into low and high frequency components without duplicating information. These functions, only requires subtractions and additions for their forward and inverse transforms. Examples of these transforms are the Discrete Fourier Transform (DFT), the Discrete Cosine Transform (DCT), the Discrete Wavelet Transforms (DWT) [21]. DWT have the advantage of representing a fundamental tool for local spectral decomposition and nonstationary signal analysis, used in the JPEG2000 standard as wavelet-based compression algorithms [22]. DWT represents an image as a sum of wavelet functions, with different location and scale [23] i.e., High-pass (detail) and Low-pass (approximate) coefficients. Low-Pass (LP) and High-Pass (HP) filters are applied to the input data with a two level signal decomposition architecture, as depicted in Figure 2.

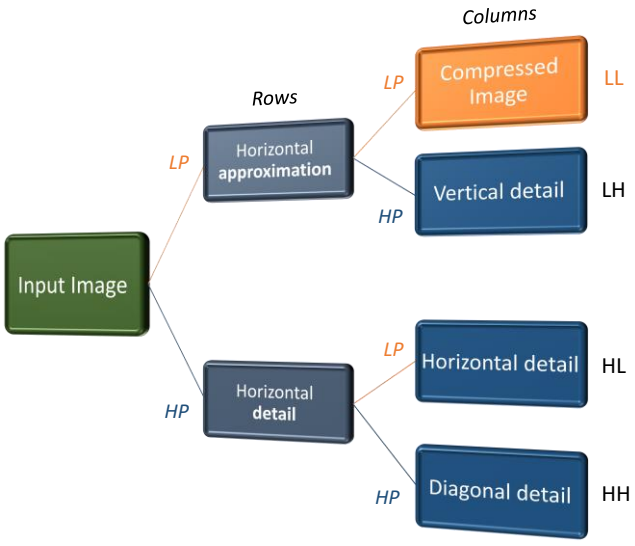

Figure 2. Two level band decomposition using multi-resolution analysis based on wavelet transform. Low-Pass (LP) and High-Pass (HP) filters are applied two times to obtain the 1D transform (L and H component) and the 2D transform with the four LL, LH, HL and HH components.

The Haar wavelet transforms [6], [24], [25] (an example of multiresolution analysis) was chosen due to their simplicity and fast computation. The sub-band decomposition achieved through the wavelet transform enables the compression directly on a specific portion of the spectrum, through spatial frequency characterization.

The all-optical system architecture for data compression based in the HT can be divided in four main building blocks: i) optical sensors array; ii) Haar wavelet transform; iii) compression; and iv) data encoding section. The scheme for all-optical image acquisition, processing, and transmission is depicted in Figure 3.

The first building block entails the acquisition stage with optical sensors for light detection and 2D data sampling. The Haar transform is implemented in the second building block, to extract the image properties by exploiting the energy compaction features of the wavelet decomposition.

The HT block (second building block) includes Low-pass (L) and High-pass (H) filters associated with the Haar wavelet, applied over one dimension (1D) at time. The filtering operation can be simplified as the calculation of the average between two neighbors' pixels values (LP) or the difference between them (HP). Equation (1) presents the Haar transform scattering matrix for a generic 1D input (a_i coefficients), i.e., pixel line or column. LP and HP filters are applied two times to obtain the 1D transform (L and H component) and the 2D transform with the four LL, LH, HL and HH components, see Figure 2 and Figure 3.

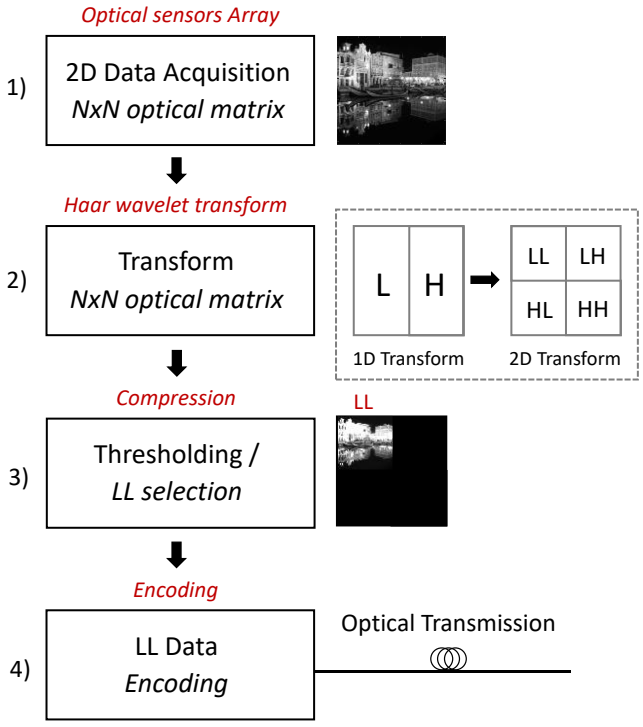

Figure 3. All-optical scheme of system building blocks for Haar wavelet transform processing and compression. 2D transform process schematic describes Low-pass (L) and High-pass (H) filtering through sub-band decomposition [6].

The coefficients on the left side of (1) are the scaling c_{ij} and detail d_{ij} coefficients (where i refers to the transform level and j to the coefficient index) obtained from the LP and HP filtering, respectively, for each pixel pair, which corresponds to the 1D first level of the Haar discrete wavelet transform. In a two dimensional (2D) matrix input ($N \times N$) this operation is performed twice, i.e., horizontally and vertically, for each transformation level, to guarantee that image intensity variations are evaluated along the two dimensions.

$$\begin{bmatrix} \vdots \\ c_{10} \\ d_{10} \\ c_{11} \\ d_{11} \\ c_{12} \\ d_{12} \\ \vdots \end{bmatrix} = \frac{1}{\sqrt{2}} \begin{bmatrix} \cdots & & \cdots & & \cdots \\ & 1\ 1\ 0 & & 0\ 0\ 0 & \\ & 1{-}1\ 0 & & 0\ 0\ 0 & \\ & 0\ 0\ 1 & & 1\ 0\ 0 & \\ \vdots & & & & \vdots \\ & 0\ 0\ 1 & & -1\ 0\ 0 & \\ & 0\ 0\ 0 & & 0\ 1\ 1 & \\ & 0\ 0\ 0 & & 0\ 1{-}1 & \\ \cdots & & \cdots & & \cdots \end{bmatrix} \begin{bmatrix} \vdots \\ a_0 \\ a_1 \\ a_2 \\ a_3 \\ a_4 \\ a_5 \\ \vdots \end{bmatrix} \quad (1)$$

In the next transform levels is performed the same filtering operation only in the LL sub-band, whereas the other sub-bands (i.e., LH, HL and HH) can be stored, transmitted or discarded, being the transform coefficients related to higher-frequency components.

The third building block carries out the compression and extracts the desirable information from the 2D transform, e.g., LL component. The all-optical system ends with the encoding building block where the data stream is delivered through the optical channel [6].

The optical device chosen to implement the HT was a 3dB asymmetric coupler, also known as a Magic-T, depicted in Figure 4.

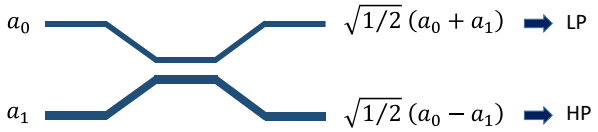

Figure 4. Scheme of a 3dB asymmetric optical coupler.

The asymmetric coupler is characterized by having different waveguides widths which can present a wide range of coupling ratios and low value of excess loss (0.7dB), including input and output single-mode fiber coupling losses [26]. To perform the HT operations the asymmetric coupler must be designed in order to perform a 50% coupling ratio.

B. PIC design for data compression

A data compression chip based on Haar wavelet transform was designed in accordance with the rules and using building blocks available from "Application Specific Photonic Integrated Circuit" (ASPIC) foundries [27], as well as proprietary building blocks created and simulated by the authors [3]. The chip was fabricated through a Multi-Project Wafer (MWP) offered by the consortium "Joint European Platform for Indium Phosphide based Photonic Integration of Components and Circuits" (JePPIX) [28]. This platform allows the development of low-cost ASPIC using generic foundry model and it supplies design kits for MPWs. The

fabrication process was achieved under the program "Photonic Advanced Research and Development for Integrated Generic Manufacturing" (PARADIGM) [29], developed to allow Universities to access to foundry processes. This program reduces the costs of the design, development and manufacture by establishing library-based design combined with technology process flows and design tools.

1) Asymmetric adiabatic coupler

An asymmetric adiabatic coupler in Indium Phosphide (InP) platform, based on adiabatic coupling arrangement was designed using the medium-index-contrast waveguide E600 structure, provided from Fraunhofer Gesellschaft Heinrich Hertz Institute (FhG-HHI) design manual structures [30]. Due to non-disclosure agreement (NDA) of Oclaro and HHI generic foundry processes, further details about the waveguide structure (e.g., structure dimensions and refractive indexes) cannot be provided. The wavelength supported by the developed structure is infrared C-band.

To achieve the phase and coupling ratios necessary for the asymmetric coupler requirements, extensive simulations and fine tuning of all design parameters were performed to attain the right profiles and outputs. Design and propagation analysis was conducted under the Beam Propagation Method (BPM) in OptoDesigner, a tool provided by Phoenix Software [31], [32]. The generic design of the developed InP asymmetric coupler is depicted in Figure 5.

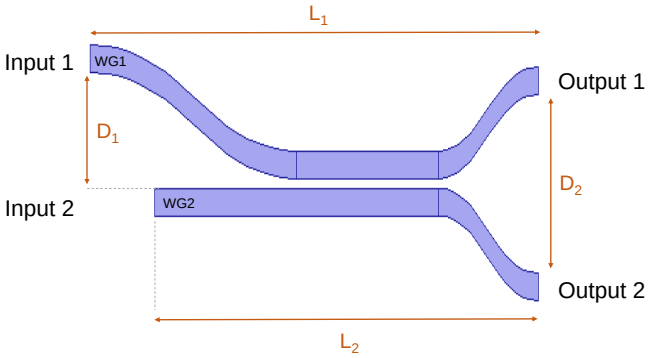

Figure 5. Diagram of the InP asymmetric adiabatic coupler composed by several sections of different sizes. The scheme diagram is not in scale.

A set of several sections of different sizes was applied in the waveguides design to guarantee the expected coupler behavior.

TABLE I. GENERAL DIMENSION S OF THE ASYMMETRIC COUPLER

	Coupler dimensions	**(μm)**
D_1	Distance between input WG	40
D_2	Distance between output WG	70
L_1	Length of WG1	2815
L_2	Length of WG2	2264

WG: Waveguides. WG1: Top waveguide from the coupler (waveguide 1). WG2: Bottom waveguide from the coupler (waveguide 2).

A summary of the general dimensions of the coupler is presented in Table I.

The waveguides were composed by a set of different sections, such as straight, taper, and bend elements [33], as depicted in Figure 6.

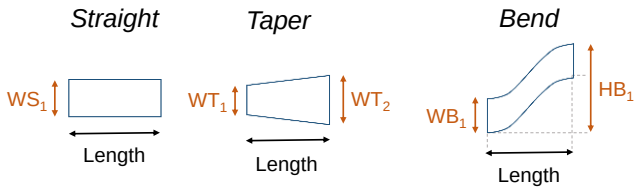

Figure 6. Diagram of three general elements that compose the different sections of the asymmetric coupler waveguide. The *taper* element is also applied in the mirror form, i.e., input as WT_2 and output as WT_1. The scheme diagram is not in scale.

The general dimensions of the elements provided in Figure 6 are presented in Table II.

TABLE II. GENERAL DIMENSIONS OF THE ELEMENTS THAT COMPOSE THE DIFFERENT SECTIONS OF THE ASYMMETRIC COUPLER

	Waveguide elements dimensions	**(μm)**
WS_1	Width of the *straight* element	1.15
WT_1	Input width of the *taper* element for WG1	1.30
	Input width of the *taper* element for WG2	1.00
WT_2	Output width of the *taper* element for WG1 and WG2	1.15
WB_1	Width of the *bend* element	1.15
HB_1	Height of the *bend* element for WG1	5.00
	Height of the *bend* element for WG2	3.60

WG: Waveguides. WG1: Top waveguide from the coupler (waveguide 1). WG2: Bottom waveguide from the coupler (waveguide 2).

To perform the Haar wavelet transform a two stages network with 3 asymmetric couplers was designed, as depicted in Figure 7.

2) Chip design

A InP data compression chip to address the Haar wavelet transform was designed [3].

The optical chip is composed by four Distributed Feedback (DFB) lasers (L1-L4), three asymmetric couplers (C1-C3), six PIN photodiodes for network monitoring two spot size converters, six multimode interferometers (MMI) 1×2 and one MMI 2×2.

The PIC includes one coupler network for compression and another one for decompression. The compression network is composed by the three asymmetric adiabatic couplers, arranged in a two stage network (as depicted in Figure 7).

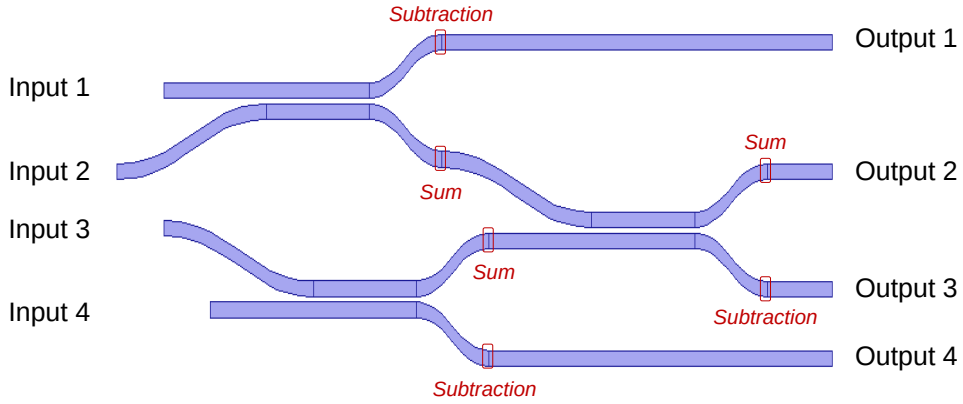

Figure 7. Diagram of the two stages network composed by three InP asymmetric adiabatic couplers to perform the expect operations of the Haar wavelet transform.

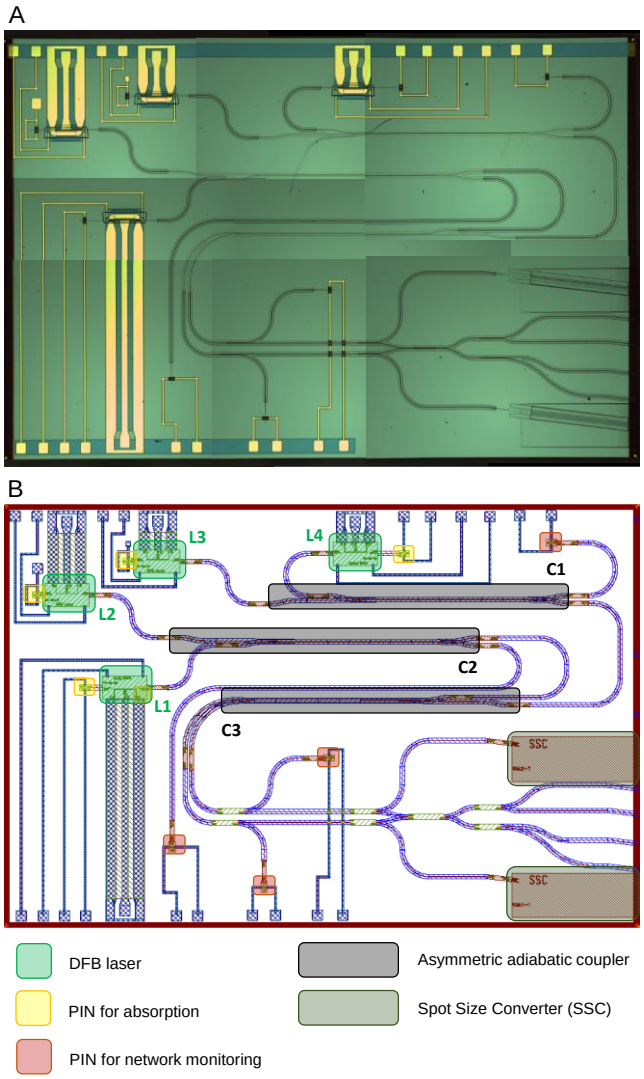

Figure 8. **A:** Microscope image of the optical chip (with objective of 5×). **B:** Design architecture of optical chip for data compression based on Haar wavelet transform.

The inputs of the compression network are fed by four DFB lasers. The outputs are connected to two spot size converters (providing optical output signal) and PIN photodiodes (providing electrical output signal), see Figure 8.

The decompression network is composed by four MMI 1×2 and one MMI 1×1. Four optical outputs are provided, as depicted in the bottom right corner of Figure 8–B.

The complete circuit architecture is presented in Figure 8.

The HT operations include Low-pass (L) and High-pass (H) filters applied over one dimension at a time. This filtering operation corresponds to the calculation of the average between two neighbors' pixels values (LP) or the difference between them (HP) [6]. The HT is implemented with a two stage network composed by three asymmetric adiabatic couplers (2×2), reproducing the required operations, i.e., the average (sum) and the difference (subtraction) between the optical input pair [3].

The 2D HT can be decomposed in 4 sub-bands, LL, LH, HL and HH [6]. The LL gives the data compressed. In the chip these 4 sub-bands can be extrapolated from the 4 output waveguides (WG) at the end of the three asymmetric couplers network, as depicted in Figure 9.

The measurements of the distance between the 4 WG at the end of the three asymmetric coupler network are $d_1 = 241.3\mu m$, $d_2 = 278.6\mu m$, and $d_3 = 248.0\mu m$, see Figure 9. Measurements were performed with a Leica microscope (DM 750M; 1CC50 HD) and an objective of 20× (HI Plan EPI, 20×/0.40) [34].

BPM simulations from OptoDesigner of the asymmetric adiabatic coupler and the two stage network are provided in *Results* subsection *A*.

C. Generation of the CGH

The CGH produces a phase mask or diffractive optical element to apply to the SLM [16]. The information to be transformed (in the Fourier domain) is introduced into the optical system by the SLM, with a phase mask that is appropriate to the input function of interest [35].

The following calculations applied for the generation of the CGH were based in the Fourier optical principles presented in [35].

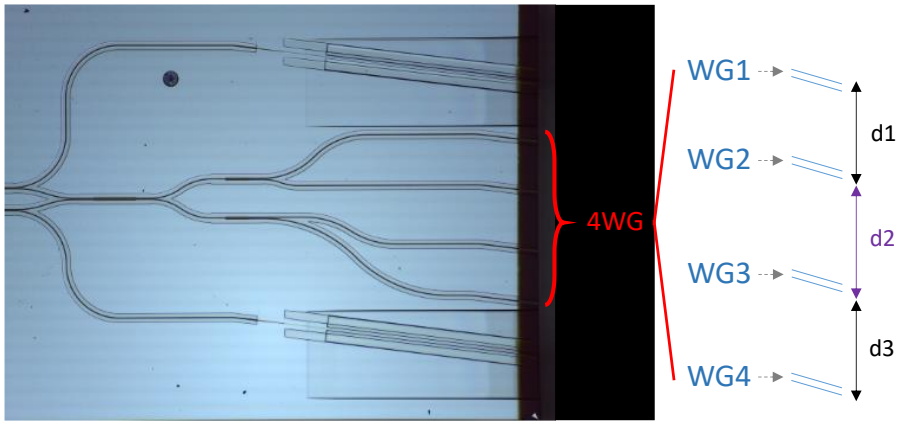

Figure 9. Measurements of the distance between the 4 waveguides (WG) at the end of the two stage compression network.

The CGH was obtained with a linear phase mask calculated in the frequency domain (1), where c_x and c_y are the horizontal and vertical tilt parameters, respectively; and f_x and f_y are the spatial frequency matrix arrays corresponding to the image to be generated in the X and Y axis, respectively.

$$Mask_{linear} = -2\pi\left(c_x\, f_x + c_y\, f_y\right) \quad (1)$$

The mask transfer function to be sent to the SLM, is given by $H_{mask} = \angle\left(\exp(iMask_{linear})\right)$, ensuring that the phase values are set in the range of $[-\pi, \pi]$.

An estimation of the output signal is given by (2).

$$S_{out} = ifft\left(H(fft(S_{in})\right) \quad (2)$$

$$S_{in} = \exp\left(-\left(2\frac{x - x_0}{wx\, log(\sqrt{2})}\right)^2 - \left(2\frac{y - y_0}{wy\, log(\sqrt{2})}\right)^2\right) \quad (3)$$

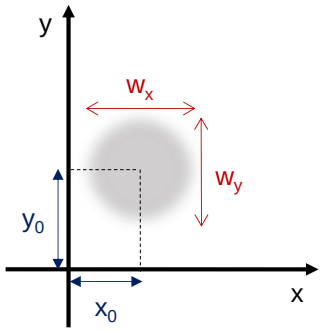

Figure 10. Diagram in Cartesian coordinate system describing the parameters (x_0, y_0) and (w_x, w_y) used for the estimation of the Input beam S_{in}.

S_{in} describes the signal of the input beam (3), where (x_0, y_0) provides the horizontal and vertical position and (w_x, w_y) the width and the height of the beam, respectively, as depicted in Figure 10.

1) *Optimization of the CGH*

To obtain a hologram that replicates the output of the 4 WG of the optical chip (see Figure 2), the linear transformations in the Fourier domain presented in (4), (5) were applied.

$$H = \angle(e^{iH_1} + e^{iH_2} + e^{iH_3} + e^{iH_4}) \quad (4)$$

$$H_1 = \exp\left(i2\pi\left(c_{x1}f_x + c_{y1}f_y\right)\right) \quad (5)$$

A phase-only SLM does not allow to simply address the inverse Fourier of the desired pattern into the far-field and replicate the resulting distribution of amplitude and phase directly on the SLM [12], thus it is challenging to spatially modulate the light with the expected resolution and accuracy.

To overcome this difficulty, an iterative algorithm to obtain the desired hologram with an error factor $\delta \leq 10\%$ was implemented. The main steps of the algorithm can be described as:

i) generate a 1st linear phase mask to produce the expected initial field (I_{exp}) based on (4);

ii) initially set the four values a_{1-4} to 1, from $H = \angle\left(a_1 e^{iH_1} + a_2 e^{iH_2} + a_3 e^{iH_3} + a_4 e^{iH_4}\right)$;

iii) acquire the hologram generated by SLM (I_{SLM}) with a camera and feed this data to the algorithm; iv) calculate the difference between the hologram generated and the initial field expected, defined as error factor: $\delta = abs(I_{SLM} - I_1) \leq 0.1$;

iv) if the condition $\delta \leq 0.1$ is not satisfied repeat steps (ii-iv) by iteratively adjusting the values of a_{1-4} to compensate the error factor. The algorithm developed in Matlab [36] was able to control both SLM and camera hardware. The block diagram of the algorithm is presented in Figure 11.

The error factor (δ) reproduces the deviation of the generated hologram when compared swith the expected output of the optical chip, i.e., the dimensions of the 4 WG.

D. *Setup to generate the CGH*

A reflective LCoS phase only SLM, model PLUTO-TELCO-012, with a wavelength range of 1400-1700 nm, an active area of 15.36 mm × 8.64 mm, a pixel pitch of 8.0 µm, a fill factor of 92% and reflectivity of 80% [10] was used to generate the hologram.

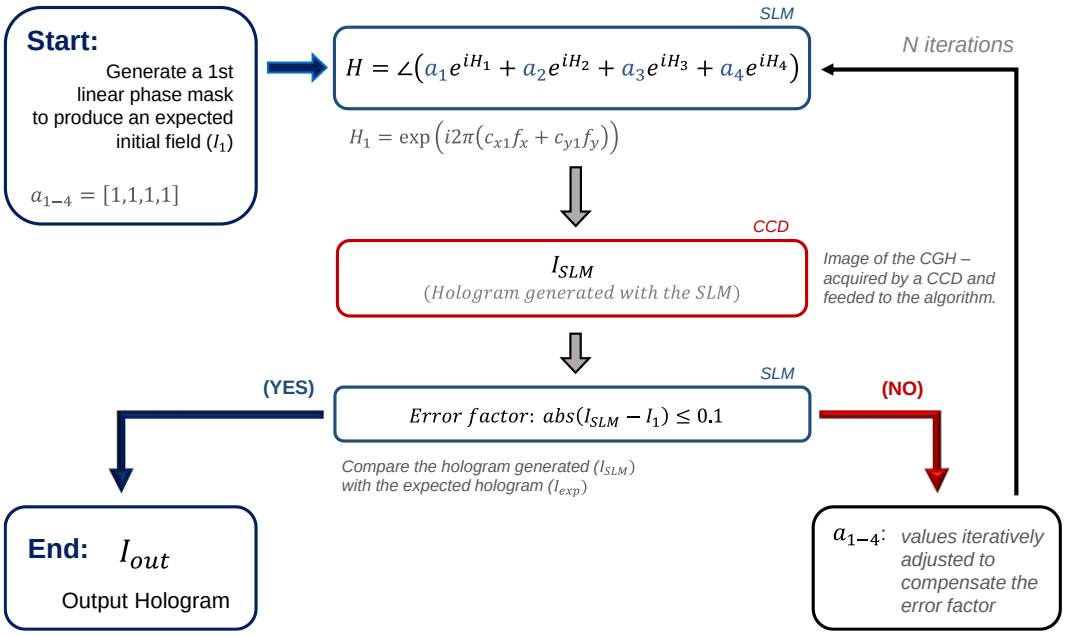

Figure 11. Block diagram of the algorithm applied for the optimization of the CGH.

The setup was composed by: a laser (1550nm wavelength); a polarization controller; two lenses (AC254-050-C-ML, AR coating 1050-1620nm) L1 and L2 with a focal length of 75mm and 250mm, respectively; a Near-Infrared (IR) (1460-1600nm) camera (sensing area: 6.4×4.8mm, resolution: 752×582, pixel size: 8.6×8.3µm) to capture the hologram produced; and a neutral density to avoid saturation in the camera acquisition, see Figure 12.

III. Results

The results section is divided in two subsections: (A) the BMP simulation results for the asymmetric adiabatic coupler; and (B) the experimental CGH results.

A. *BPM simulations*

Light propagation simulations of the InP asymmetric adiabatic coupler with input signal in the: i) upper waveguide (WG1); ii) lower waveguide (WG2); and iii) same input signal in both WG1 and WG2; are presented in Figure 13.

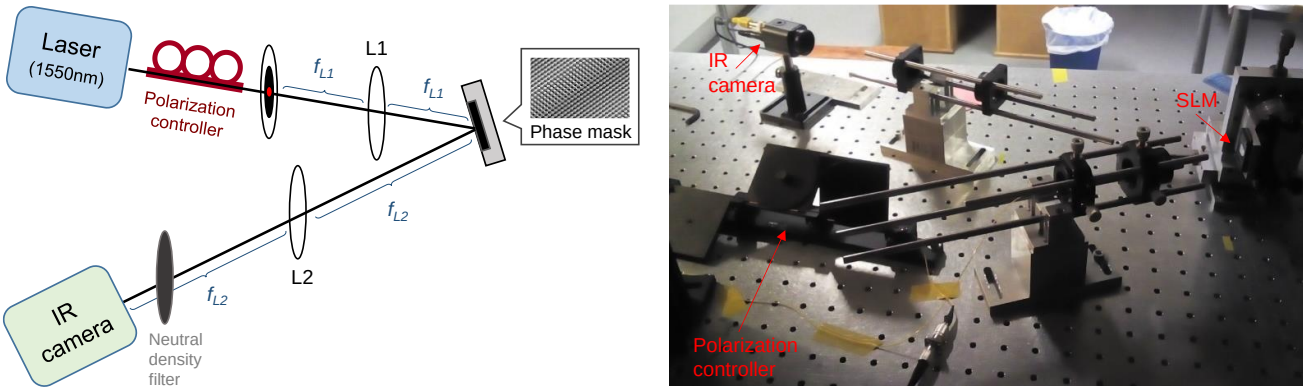

Figure 12. Left figure: Scheme of the hologram reconstruction system, using a laser of 1550nm, a polarization controller, lens L1, a LCoS-SLM, lens L2 and a IR camera. Right figure: Photography of the setup presented in the left figure.

The power propagation result for the two stage network composed by three asymmetric adiabatic couplers is presented in Figure 13.

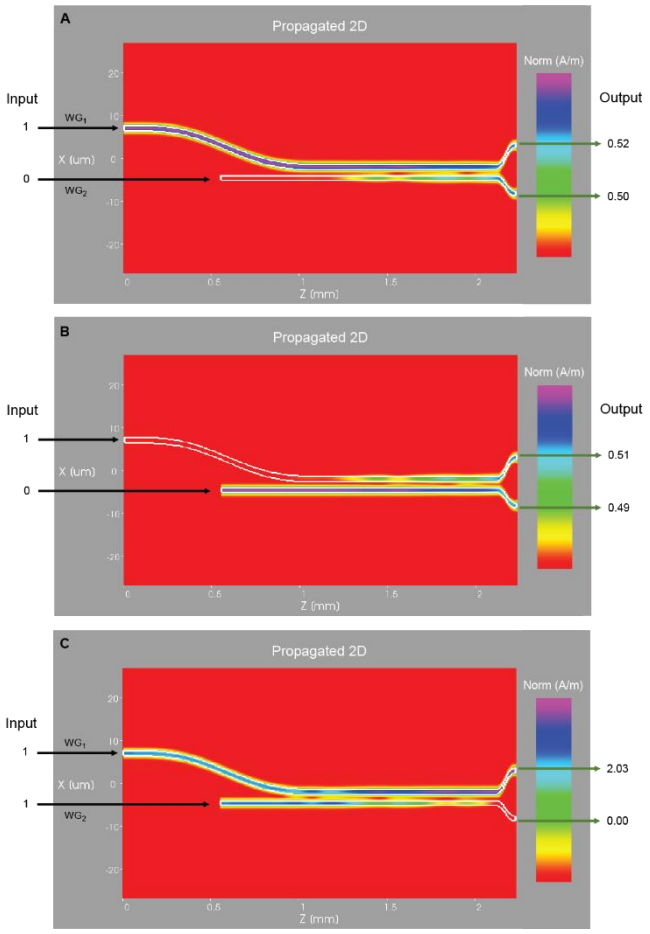

Figure 13. Power propagation in the asymmetric adiabatic coupler when fed with signal on: (A) upper waveguide (WG1), (B) lower waveguide (WG2), (C) both WG1 and WG2.

The simulation results demonstrate that the coupler is behaving according to expected. As depicted in Figure 13-A and Figure 13-B, the behavior as a 50% splitter is observed, when only one of the input waveguides carries an optical signal.

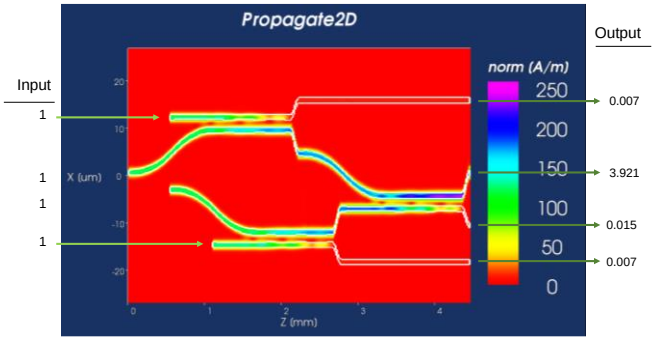

Figure 14. Power propagation for the two stage network composed by three asymmetric adiabatic couplers.

When both of the input waveguides carry an optical signal, sum and subtraction are achieved at their output waveguides. See the duplication of power in one of the waveguides and the absence of power in the other, Figure 13-C.

The obtained results for the two stage network composed by three InP asymmetric adiabatic couplers are displayed in Figure 14. As expected, the HT operations are carried out correctly, which can be confirmed by the power at the four output waveguide ports.

B. Experimental CGH results

A hologram was generated in 1st order of diffraction where the polarization was occurring.

Figure 15. Hologram acquired by the IR camera, left: initial CGH; right: CGH optimized.Figure 15 presents the holograms acquired by the IR camera, i.e., the initial hologram (I_1) fed to the optimization algorithm and the final optimized hologram (I_{out}).

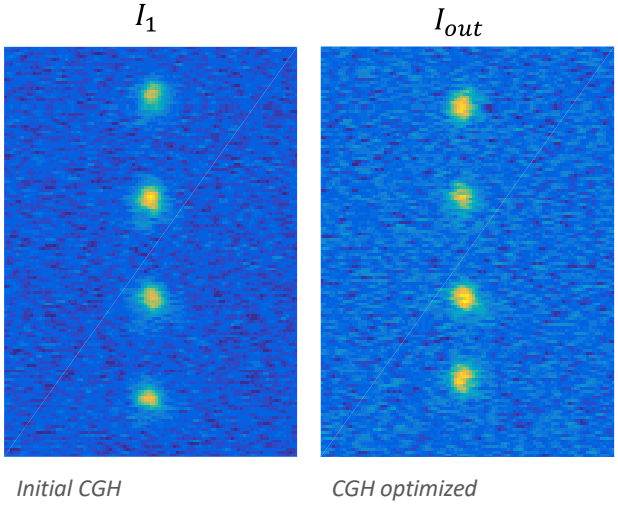

Figure 15. Hologram acquired by the IR camera, left: initial CGH; right: CGH optimized.

The analysis of the obtained hologram image can be described by the following steps:

(1) Calculate the intensity integration of the hologram, i.e. sum of all elements along each line of the image matrix, depicted as S_{raw};
(2) application of the Savitzky-Golay (SG) filter to smooth the intensity integration signal obtained in step (1), depicted as S_{SG};;
(3) implementation of a first order Gaussian fit curve to the filtered signal, depicted as *Gauss fit*;
(4) extraction of Gaussian parameters to calculate the spots distances, i.e., obtained from the holograms versus expected results (d_1, d_2 and d_3 from the optical chip).

The signal smoothing of the intensity integration was obtained with the Savitzky-Golay filter, which can be characterized by a generalized moving average with filter coefficients determined by an unweighted linear least-squares regression and a polynomial model of specified degree [36].

The parameters applied in the filter were a polynomial order 9 and a window length 19.

Results after steps (1) and (2) are depicted in Figure 16.

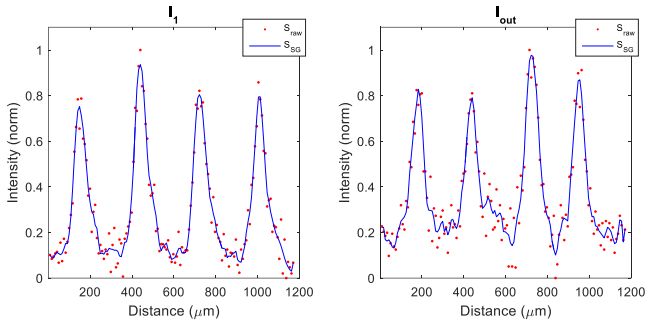

Figure 16. Integrated intensity from the hologram image S_{raw} (red dots), and correspondent smoothing with Savitzky-Golay (SG) filter S_{SG} (blue line). Left: Initial CGH; Right: Optimized CGH.

Results from Gaussian curve fitting application are presented in Figure 17.

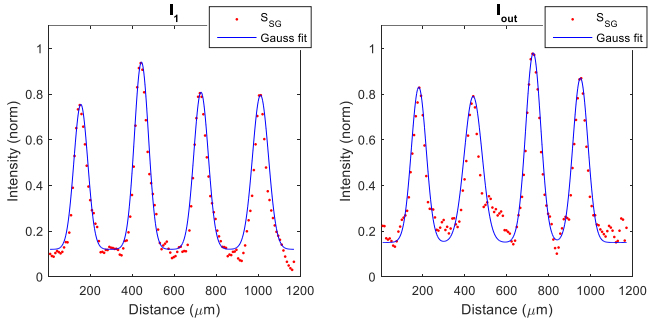

Figure 17. Gaussian fit (*Gauss fit* – blue line) of smoothed integrated intensity signal from the hologram image (S_{SG} – red dots). Left: Initial CGH; Right: Optimized CGH.

The distance between the spots was calculated from the center position of each spots, given by the Gaussian fit coefficient correspondent to the position of the center of the peak. The coefficients were obtained with 95% confidence bounds.

TABLE III. ERROR FACTOR (δ) VALUES FOR d_1, d_2, AND d_3

	Initial CGH	**Optimized CGH**
δ_{d1}	0.20	0.07
δ_{d2}	0.02	0.03
δ_{d3}	0.14	0.09

The deviation values (δ) of the generated hologram (i.e., initial I_1 and optimized I_{out} holograms) when compared with the expected output of the optical chip (i.e., d_1, d_2 and d_3 from Figure 9) are presented in Table III.

An error factor $\delta \leq 20\%$ was obtained for the initial CGH and $\delta \leq 9\%$ for the final optimized CGH.

IV. DISCUSSION

The design of the asymmetric adiabatic coupler and the all-optical network implemented to perform the Haar wavelet transform in InP were demonstrate to operate according to predictions as confirmed by the BPM simulations, supporting their feasibility for compression purposes.

An improvement in the generated hologram is achieved with CGH optimization, i.e., a major reduction of 11% (difference between initial and optimized) in the error factor (δ) was obtained. Nevertheless, optical artefacts associated with the diffraction of light were not completely eliminated, i.e., additional 2 spots (with less intensity) are generated. This diffraction artefact can cause a reduction of signal expected at the 4 output WG of the optical chip.

The phase mask that replicates the expected output of the optical chip can be used to multiplex/demultiplex the obtained result. Furthermore, a phase mask which addresses the HT operations can also be applied to invert the compression induced by the HT (optically implemented in the chip with the 3 asymmetric couplers network). The use of the SLM will allow to provide a proof of concept of the PIC operation.

V. CONCLUSION

An extensive PIC characterization and testing is essential to provide an accurate prediction of its performance. In this study, we proposed a concept to use the SLM as a flexible platform for feeding photonic integrated processors in order to complement the PIC characterization process. The capacity of the SLM to dynamically reconfigure light allows to feed and/or receive information to the PIC. This data can be used to provide a proof of concept of the operation performed by the optical chip, e.g., 2D HT. The design of building blocks for the HT implementation as well as the all-optical network were proposed and simulated, demonstrating their viability for compression. A first result was obtained, i.e., a phase mask that can be used to feed/receive the output of an optical chip for data compression based in the HT.

ACKNOWLEDGMENT

This work is funded by Fundação para a Ciência e a Tecnologia (FCT) under through national funds under the scholarships PD/BD/105858/2014 and SFRH/BPD/119188/2016; and the project COMPRESS - All-optical data compression – PTDC/EEI-TEL/7163/2014. Additional support was provided by the European Regional Development Fund (FEDER), through the Regional Operational Program of Centre (CENTRO 2020) of the Portugal 2020 framework [Project HeatIT with Nr. 017942 (CENTRO-01-0247-FEDER-017942)], and the COST action CA16220 European Network for High Performance Integrated Microwave Photonics (EUIMWP). The authors acknowledge PICadvanced for its collaboration.

REFERENCES

[1] Grand View Research, "Photonic Integrated Circuit (IC) Market Size Report," 2016.

[2] Credence Research, "Photonic Integrated Circuits Market,"

2016.

[3] C. Pinho *et al.*, "Design and Characterization of an Optical Chip for Data Compression based on Haar Wavelet Transform," in *OFC - Optical Networking and Communication Conference*, 2017, p. Th2A.9.

[4] M. Smit *et al.*, "An introduction to InP-based generic integration technology," *Semicond. Sci. Technol.*, vol. 29, no. 8, p. 83001, 2014.

[5] V. Ashok, T. Balakumaran, C. Gowrishankar, I. L. A. Vennila, and A. N. Kumar, "The Fast Haar Wavelet Transform for Signal & Image Processing," *Int. J. Comput. Sci. Inf. Secur.*, vol. 7, no. 1, pp. 126–130, 2010.

[6] G. Parca, P. Teixeira, and A. Teixeira, "All-optical image processing and compression based on Haar wavelet transform," *Appl. Opt.*, vol. 52, no. 12, pp. 2932–2939, 2013.

[7] J. Carpenter, S. Leon-saval, B. J. Eggleton, and J. Schröder, "Spatial Light Modulators for Sub-Systems and Characterization in SDM," in *2014 OptoElectronics and Communication Conference and Australian Conference on Optical Fibre Technology*, 2014, no. July, pp. 23–24.

[8] H. J. Lee, H. S. Moon, S.-K. Choi, and H. S. Park, "Multi-core fiber interferometer using spatial light modulators for measurement of the inter-core group index differences," *Opt. Express*, vol. 23, no. 10, p. 12555, May 2015.

[9] Meadowlark Optics, "XY Spatial Light Modulator," 2015. [Online]. Available: http://www.meadowlark.com/xy-spatial-light-modulator-p-119#.VfLwdhFVhHx. [Accessed: 01-Aug-2016].

[10] Holoeye, "Spatial Light Modulators," *Holoeye Photonics AG*, 2013. [Online]. Available: http://holoeye.com/spatial-light-modulators/. [Accessed: 01-Aug-2016].

[11] Department of Physics, "An Introduction to Spatial Light Modulators," *Stony Brook University*, 2013. [Online]. Available: http://laser.physics.sunysb.edu/~melia/SLM_intro.html. [Accessed: 03-Sep-2014].

[12] J. Carpenter, "Holographic Mode Division Multiplexing in Optical Fibres," University of Cambridge, 2012.

[13] G. Lazarev, A. Hermerschmidt, and S. Kr, "LCOS Spatial Light Modulators : Trends and Applications," *Opt. Imaging Metrol. Adv. Technol.*, pp. 1–29, 2012.

[14] Hamamatsu, "Phase spatial light modulator LCOS-SLM," in *Handbook LCOS-SLM*, 2012, pp. 1–14.

[15] M. Kovachev *et al.*, "Reconstruction of Computer Generated Holograms by Spatial Light Modulators," *Multimedia Content Representation, Classification and Security*, vol. 4105. Springer Berlin Heidelberg, pp. 706–713, 2006.

[16] C. Pinho, A. Shahpari, I. Alimi, M. Lima, and A. Teixeira, "Optical transforms and CGH for SDM systems," in *2016 18th International Conference on Transparent Optical Networks (ICTON)*, 2016, pp. 1–4.

[17] Y. Torii, L. Balladares-Ocana, and J. Martinez-Castro, "An Iterative Fourier Transform Algorithm for digital hologram generation using phase-only information and its implementation in a fixed-point digital signal processor," *Optik (Stuttg).*, vol. 124, no. 22, pp. 5416–5421, 2013.

[18] O. Ripoll, V. Kettunen, and H. P. Herzig, "Review of iterative Fourier-transform algorithms for beam shaping applications," *Opt. Eng.*, vol. 43, no. 11, pp. 2549–2556, 2004.

[19] R. Gerchberg, W. O. Saxton, B. R. W. Gerchberg, and W. O. Saxton, "A Practical Algorithm for the Determination of Phase from Image and Diffraction Plane Pictures," *Optik (Stuttg).*, vol. 35, no. 2, pp. 237–246, 1972.

[20] J. Carpenter and T. D. Wilkinson, "Graphics processing unit–accelerated holography by simulated annealing," *Opt. Eng.*, vol. 49, no. 9, pp. 95801–7, 2010.

[21] K. Deb, M. S. Al-Seraj, M. M. Hoque, and M. I. H. Sarkar, "Combined DWT-DCT based digital image watermarking technique for copyright protection," in *7th International Conference on Electrical and Computer Engineering*, 2012, pp. 458–461.

[22] C. Christopoulos, A. Skodras, and T. Ebrahimi, "The JPEG2000 still image coding system: an overview," *IEEE Trans. Consum. Electron.*, vol. 46, no. 4, pp. 1103–1127, 2000.

[23] K. S. Thyagarajan, *Still Image and Video Compression with MATLAB*. Hoboken, NJ, USA: John Wiley & Sons, Inc., 2011.

[24] M. Vetterli, J. Kovačević, and V. K. Goyal, *Foundations of signal processing*. 2014.

[25] J. Kovacevic, V. K. Goyal, and M. Vetterli, *Fourier and Wavelet Signal Processing*, no. October. 2013.

[26] A. Takagi, K. Jinguji, and M. Kawachi, "Design and fabrication of broad-band silica-based optical waveguide couplers with asymmetric structure," *IEEE J. Quantum Electron.*, vol. 28, no. 4, pp. 848–855, Apr. 1992.

[27] G. Gilardi and M. K. Smit, "Generic InP-Based Integration Technology : Present and Prospects," *Progress In Electromagnetics Research*, 2014. [Online]. Available: http://www.jpier.org/PIER/pier147/02.14022001.pdf. [Accessed: 04-Feb-2015].

[28] JePPIX, "Joint European Platform for InP-based Photonic Integrated Components and Circuits." [Online]. Available: http://www.jeppix.eu.

[29] PARADIGM, "Photonic Advanced Research and Development for Integrated Generic Manufacturing," *May 29, 2014, PARADIGM and EuroPIC consortia*. [Online]. Available: http://www.paradigm.jeppix.eu/.

[30] PARADIGM, "Photonic Advanced Research and Development for Integrated Generic Manufacturing," *May 29, 2014, PARADIGM and EuroPIC consortia*. .

[31] Phoenix Software, "OptoDesigner 5 - The ultimate Photonic Chip Design environment," 2016. [Online]. Available: http://www.phoenixbv.com/product.php?submenu=dfa&subsubmenu=3&prdgrpID=3. [Accessed: 12-Sep-2016].

[32] PhoeniX Software, "User Manual OptoDesigner - version 5.0.7." p. 1825, 2015.

[33] PhoeniX BV, "User Manual OptoDesigner PhoeniX Software, version 5.1.4." p. 2913, 2017.

[34] Leica Microsystems, "Leica Application Suite," *Http://Www.Leica-Microsystems.Com/*, 2015. [Online]. Available: http://www.leica-microsystems.com/products/microscope-software/life-sciences/las-easy-and-efficient/. [Accessed: 04-Sep-2016].

[35] J. W. Goodman, *Introduction to Fourier Optics*, 2nd ed. 1996.

[36] The MathWorks, "MATLAB - The language of technical computing." 2015.